Pulsed Acceleration Charge Detection Mass Spectrometry: Application to Weighing Electrosprayed Droplets

Sarah R. Mabbett, Lloyd W. Zilch, Joshua T. Maze, John W. Smith, and Martin F. Jarrold*

Chemistry Department, Indiana University, 800 East Kirkwood Avenue, Bloomington, Indiana 47405

We describe a new approach to measuring the masses of individual macroions. The method employs a pulsed acceleration tube located between two sensitive image charge detectors. The charge and velocity of the macroion are recorded with the first image charge detector. The ion is pulse accelerated through a known voltage drop, and then the charge and velocity are remeasured using the second image charge detector. The mass of the ion is deduced from its charge and its initial and final velocities. The approach has been used to measure masses in the 10^{10}−10^{14} Da range with $z = 10^3$−10^6 and $m/z = 10^6$−10^9. It should be extendable to masses of $<10^6$ Da. We have used the method to determine the size and charge of water droplets transmitted through a capillary interface and an aperture interface. The droplets detected from the aperture interface are ~1 order of magnitude smaller in mass than those detected from the capillary interface. The droplets from both interfaces have relatively low charges, particularly with the capillary interface where they are only charged to a small fraction of the Rayleigh limit. These results suggest that the aerodynamic breakup of the droplets plays a significant role in the mechanism of electrospray ionization.

There is interest in determining the masses of large ions for many reasons. Noncovalent complexes like ribosomes and viruses can be transferred to the gas phase by electrospray, where they can, in principle, be analyzed by mass spectrometry. Measuring the masses of nanoparticles would provide an easy way to determine their size distribution. However, the conventional methods of doing mass spectrometry start to become inadequate as the mass approaches several hundred kilodaltons. The electrospray mass spectrum for a single species consists of a series of peaks corresponding to different charge states, and it is necessary to deduce the charge to determine the mass. For a small species, there are only a few charge states and the charges and the mass can be obtained quite easily. As the mass increases, the charge and the number of charge states increases; nevertheless, it is still possible to determine the mass as long as the individual charge states are resolved. However, for large ions, each charge state often has a distribution of masses due to incomplete dehydration, residual counterions, or intrinsic heterogeneity; so the charge states are often not resolved, and the mass spectrum becomes broad and featureless.[1] Because the charge states are not resolved, the charges cannot be deduced, and so the mass cannot be determined. One way to circumvent this problem is to effectively lower the charge on the ion so that it appears at a larger m/z. Robinson, Loo, Heck, and others have used this approach to study protein complexes with masses up to, and in some cases beyond, a megadalton.[2−12] However, the detection efficiency of ions with large m/z by electron multiplier detectors is low, which hampers the extension of this approach to larger ions. Alternative detection methods have been explored, but they invariably suffer from diminished response time, which degrades the mass resolution.[13−15]

One solution to these problems is to measure m/z and z for each individual ion. With this approach, it is no longer necessary to resolve the charge states in the m/z spectrum, and so this method can be applied to very heterogeneous samples such as polymers and nanoparticles. Smith and collaborators implemented a version of this approach in the mid 1990's using Fourier

* To whom correspondence should be addressed. Phone: (812) 856-1182. Fax: (812) 855-8300. E-mail: mfj@indiana.edu.

(1) Tito, M. A.; Tars, K.; Valegard, K.; Hajdu, J.; Robinson, C. V. *J. Am. Chem. Soc.* **2000**, *122*, 3550−3551.
(2) Loo, J. A. *Mass Spectrom. Rev.* **1997**, *16*, 1−23.
(3) Rostom, A. A.; Robinson, C. V. *Curr. Opin. Struct. Biol.* **1999**, *9*, 135−141.
(4) Heck, A. J. R.; van den Heuvel, R. H. H. *Mass Spectrom. Rev.* **2004**, *23*, 368−389.
(5) Loo, J. A. *Int. J. Mass Spectrom.* **2000**, *200*, 175−186.
(6) Chernushevich, I. V.; Ens, W.; Standing, K. G. Measurement of Noncovalent Complexes with High m/z by Electrospray Time-of-Flight Mass Spectrometry. In *New Methods for the Study of Biomolecular Complexes*; Ens, W., Standing, K. G., Chernushevich, I. V., Eds.; NATO ASI Series C; Kluwer: Dordrecht, The Netherlands, 1998; pp 101−116.
(7) Benjamin, D. R.; Robinson, C. V.; Hendrick, J. P.; Hartl, F. U.; Dobson, C. M. *Proc. Natl. Acad. Sci. U.S.A.* **1998**, *95*, 7391−7395.
(8) Rostom, A. A.; Robinson, C. V. *J. Am. Chem. Soc.* **1999**, *121*, 4718−4719.
(9) Pinkse, M. W. H.; Maier, C. S.; Kim, J.-I.; Oh, B.-H.; Heck, A. J. R. *J. Mass Spectrom.* **2003**, *38*, 315−320.
(10) Van Berkel, W. J. H.; van den Heuvel, R. H. H.; Versluis, C.; Heck, A. J. R. *Protein Sci.* **2000**, *9*, 435−439.
(11) Sanglier, S.; Leize, E.; van Dorsselaer, A.; Zal, F. *J. Am. Soc. Mass Spectrom.* **2003**, *14*, 419−429.
(12) Loo, J. A.; Berhane, B.; Kaddis, C. S.; Wooding, K. M.; Xie, Y. M.; Kaufman, S. L.; Chernushevich, I. V. *J. Am. Soc. Mass Spectrom.* **2005**, *16*, 998−1008.
(13) Westmacott, G.; Zhong, F.; Frank, M.; Friedrich, S.; Labov, S. E.; Benner, W. H. *Rapid Commun. Mass Spectrom.* **2000**, *14*, 600−607.
(14) Frank, M.; Labov, S. E.; Westmacott, G.; Benner, W. H. *Mass Spectrom. Rev.* **1999**, *18*, 155−186.
(15) Wenzel, R. J.; Matter, U.; Schultheis, L.; Zenobi, R. *Anal. Chem.* **2005**, *77*, 4329−4337.

transform mass spectrometry and charge shifting.[16−18] Individual ions are isolated and the mass to charge ratio is determined as the ion undergoes charge-shifting reactions like deprotonation. The charge is then deduced from the shift in the mass to charge ratio. This approach has been implemented for ions with masses of 10^5–10^7 Da. For larger ions (10^8 Da), the charge was determined directly from the image charge induced on the detection electrodes.[19] However, the uncertainty in the charge determination is substantial in this case ($\pm 10\%$) because it requires knowledge of the radius of the cyclotron orbit, which is not amenable to direct measurement.

A related approach to determining the masses of mesoscopic objects is charge detection mass spectrometry. This approach was first developed to determine the masses of microparticles.[20,21] In this application, the microparticles are charged, accelerated, and travel through three shielded cylinders. As they travel through the cylinders, the charged particles induce an image charge, which is amplified. The size of the image charge on the long central cylinder provides a measure of the charge on the particle, and the time interval between the transients on the first and third cylinders provides a measure of the mass to charge ratio (assuming that the acceleration voltage is known). Thus, the mass of each individual microparticle can be determined and a histogram constructed. A variation of this approach was used by Benner, Fuerstenau, and their collaborators to perform mass measurements on large DNA fragments and electrosprayed viruses.[22−24]

In their implementation, the electroprayed ions are accelerated by a voltage gradient and the resulting beam travels through a single charge detection cylinder. The transit time provides a measure of the time-of-flight, and the charge is deduced from the image charge. However, the ions undergo substantial aerodynamic acceleration in the electrospray interface, leading to a broad distribution of initial velocities. This distribution limits the accuracy of the mass measurements for large m/z ions (where the velocity increment resulting from acceleration in the voltage gradient is comparable to, or less than, the aerodynamic velocity).

In the approach we employ here, we account for the aerodynamic acceleration exactly by measuring the velocity of each ion before it is pulse accelerated. We use two sensitive image charge detectors separated by a pulsed accelerator. The charge and velocity of the ion is recorded in the first image charge detector, then the ion is pulse accelerated, and the charge and velocity are remeasured in the second image charge detector. The m/z ratio is determined from the two velocity measurements and the acceleration voltage. The mass of each individual ion is then determined from its m/z ratio and its charge. In the work reported here, we use this approach to determine the size of electrosprayed water droplets transmitted through a capillary interface and an aperture interface.

The mechanism by which desolvated ions are generated by electrospray has been a topic of heated discussion. The current consensus[25−29] is that the small charged droplets generated by electrospray evaporate and shrink until they reach a point where the electrostatic forces exceed surface tension (the Rayleigh limit[30]). The droplets then discharge by emitting a jet of small highly charged droplets. This evaporative shrinking and jetting process is thought to continue until the droplets reach a sufficiently small size that isolated ions can be generated from them. The mechanism by which the ions are formed from the small droplets has been the most contentious issue in discussions of the electrospray ionization process. In the charge residue mechanism,[31,32] the evaporative shrinking and jetting continues until the progeny droplets contain only a single solute ion. The solvent then evaporates leaving behind the unsolvated ion. In the ion evaporation mechanism,[33] the strong electric field at the surface of a small droplet drives the evaporation of an ion from the droplet's surface. Little attention has been paid to how the droplets shrink to the size where ions can be formed and, in particular, to the role that aerodynamic forces in the vacuum interface may play in the breakup of the droplets.

EXPERIMENTAL METHODS

A schematic diagram of the apparatus is shown in Figure 1. Water droplets are generated by electrospray. The electrospray emitter is a polyimide-coated fused-silica capillary with 250-μm inner diameter. The emitter is coupled to a Cole-Parmer syringe pump (model EW-74900−00) that provides a constant flow of 1000 μL/h. The results reported here were obtained with HPLC-grade water (Omni-Solv, Fisher Scientific) that was degassed by sonicating under vacuum for ∼2 h before use. Purified (18.2 MΩ) and filtered (20 nm) water gave similar results. The source was operated with +4500 V applied to the water by means of an electrode that enters the liquid flow through a tee. Electrospraying occurred in the cone-jet mode. The electrosprayed droplets are transferred into vacuum through either a capillary interface or an aperture interface. The capillary interface is a stainless steel tube 12.7 cm long and with a 500-μm inner diameter. We estimate from the gas volume flow through the capillary interface that the average residence time is ∼0.5 ms. This is an upper limit. The aperture interface is a 127-μm-thick beryllium copper plate containing a 250-μm-diameter aperture. After passing through the interface, the droplets travel through two differentially pumped

(16) Smith, R. D.; Cheng, X.; Bruce, J. E.; Hofstadler, S. A.; Anderson, G. A. *Nature* **1994**, *369*, 137−139.

(17) Cheng, X.; Bakhtiar, R.; Van Orden, S.; Smith, R. D. *Anal. Chem.* **1994**, *66*, 2084−2087.

(18) Bruce, J. E.; Cheng, X.; Bakhtiar, R.; Wu, Q.; Hofstadler, S. A.; Anderson, G. A.; Smith, R. D. *J. Am. Chem. Soc.* **1994**, *116*, 7839−7847.

(19) Chen, R.; Cheng, X.; Mitchell, D. W.; Hofstadler, S. A.; Wu, Q.; Rockwood, A. L.; Sherman, M. G.; Smith, R. D. *Anal. Chem.* **1995**, *67*, 1159−1163.

(20) Keaton, P. W.; Idzorek, G. C.; Rowton, L. J.; Seagrave, J. D.; Stradling, G. L.; Bergeson, S. D.; Collopy, M. T.; Curling, H. L.; McColl, D. B.; Smith, J. D. *Int. J. Impact Eng.* **1990**, *10*, 295−308.

(21) Stradling, G. L.; Idzorek, G. C.; Shafer, B. P.; Curling, H. L.; Collopy, M. T.; Blossom, A. A. H.; Fuerstenau, S. *Int. J. Impact Eng.* **1993**, *14*, 719−727.

(22) Fuerstenau, S. D.; Benner, W. H. *Rapid Commun. Mass Spectrom.* **1995**, *9*, 1528−1538.

(23) Benner, W. H. *Anal. Chem.* **1997**, *69*, 4162−4168.

(24) Fuerstenau, S. D.; Benner, W. H.; Thomas, J. J.; Brugidou, C.; Bothner, B.; Siuzdak, G. *Angew. Chem., Int. Ed.* **2001**, *40*, 541−544.

(25) Cole, R. B. *J. Mass Spectrom.* **2000**, *35*, 763−772.

(26) Gamero-Castaño, M.; Fernandez de la Mora, J. *J. Mass Spectrom.* **2000**, *35*, 790−803.

(27) Kebarle, P. *J. Mass Spectrom.* **2000**, *35*, 804−817.

(28) Kebarle, P.; Peschke, M. *Anal. Chim. Acta* **2000**, *406*, 11−35.

(29) Cech, N. B.; Enke, C. G. *Mass Spectrom. Rev.* **2001**, *20*, 362−387.

(30) Lord Rayleigh, *Philos. Mag.* **1882**, *14*, 184−186.

(31) Dole, M.; Mack, L. L.; Hines, R. L.; Mobley, R. C.; Ferguson, L. D.; Alice, M. B. *J. Chem. Phys.* **1968**, *49*, 2240−2249.

(32) Mack, L. L.; Kralik, P.; Rheude, A.; Dole, M. *J. Chem. Phys.* **1970**, *52*, 4977−4986.

(33) Iribarne, J. V.; Thomson, B. A. *J. Chem. Phys.* **1976**, *64*, 2287−2294.
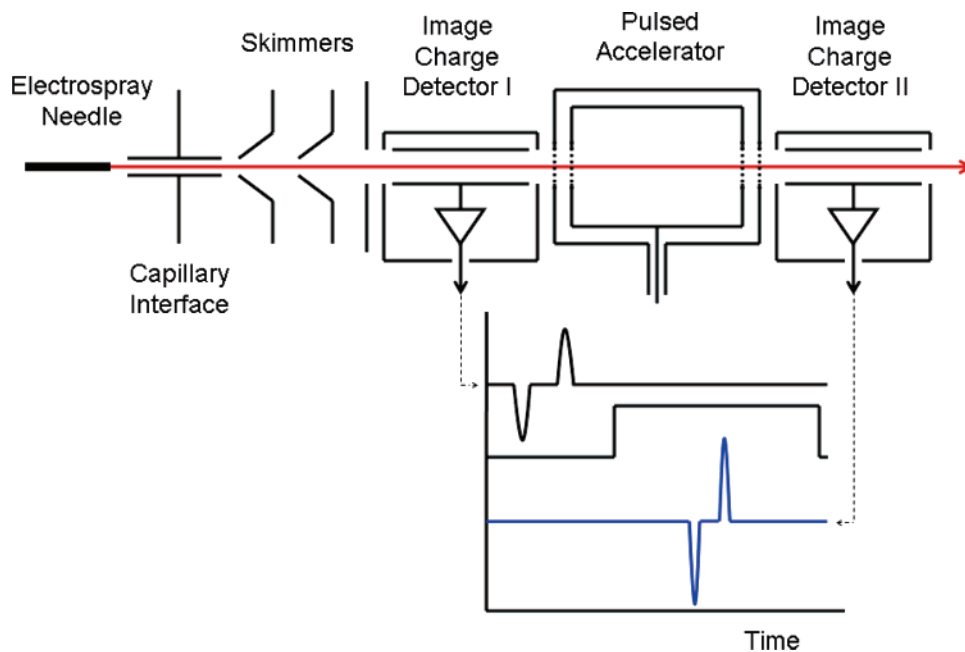
Figure 1. Schematic diagram of the experimental apparatus. The lower portion of the figure shows the signal obtained from the first image charge detector (top), the voltage applied to the pulse accelerator (middle), and the signal obtained from the second image charge detector (bottom).

regions that are separated by a conical skimmer. Another conical skimmer separates the second differentially pumped region from the analysis region. Both skimmers are grounded. The pressure in the first differentially pumped region (which is pumped by a mechanical booster pump) is ~0.40 Torr. The pressure in the second differentially pumped region is $\sim 8 \times 10^{-5}$ Torr. The pressure in the analysis region is $\sim 2 \times 10^{-6}$ Torr. The analysis region houses two image charge detectors separated by a pulsed acceleration tube. The image charge detectors and pulsed acceleration tube are aligned axially with the droplet beam. The image charge detection assemblies are modeled after the design of Fuerstenau and Benner.[22] The assemblies have a central stainless steel tube, 3.81 cm long and with an internal diameter of 0.65 cm. When charged objects pass through, an equal but opposite charge is induced on the tube. The image charge is detected by a low-noise charge-sensitive preamplifier (Amptek A250) through an external JFET (2SK152). The image charge detection tube, the JFET, and preamplifier are enclosed in a grounded stainless steel case, which has 0.5-cm diameter apertures that allow the droplets to pass through undisturbed. The signal from the preamplifier is processed by a differentiating spectroscopy amplifier (Ortec, 571) and recorded with a 16-bit transient digitizer (AlazarTech, ATS460) operated with a sampling rate of 125 MHz.

The stainless steel acceleration tube measures 15.24 cm in length and has a 1.27-cm inner diameter. The acceleration tube is enclosed in a grounded stainless steel case to prevent the electrical noise that is generated when the acceleration voltage is pulsed from reaching the image charge detectors. A stainless steel mesh is attached to both ends of the acceleration tube and over the apertures in the grounded shield. The approach used to attach the grids ensures that they are flat so that the electric fields in the acceleration region are uniform. The voltage to the acceleration tube is provided by a high-voltage pulse generator

(Directed Energy Inc., PVX-4140). As shown in Figure 1, the voltage on the acceleration tube is initially zero. When a droplet is detected entering the first image charge detector, the voltage on the acceleration tube is switched to +3500 V after a preset delay. The function of the delay is to allow the droplet to enter the grounded acceleration tube before the voltage is switched. When the droplet leaves the acceleration tube, it is accelerated across a 2.2×10^6 V/m gradient in the gap between the end of the acceleration tube and its ground shield. In the work reported here, we used a delay of 250 μs. If the delay is too long, the fast-moving droplets will exit the acceleration tube before the voltage pulse is applied. On the other hand, if the delay is too short, slow-moving droplets will not make it into the acceleration tube before the voltage pulse is applied. The velocity distribution of the droplets is relatively broad, and the value for the delay used here is a compromise to minimize the loss of fast and slow droplets. After the voltage is applied, it must remain on for a period that is long enough for the slow-moving droplets to exit. In the work reported here, we used a pulse period of 4 ms.

After acceleration, the droplets pass through the second image charge detector. The signal from the second image charge detector is processed in the same way as the signal from the first and both signals are recorded simultaneously in the transient digitizer. As noted above, the signals are processed by a differentiating amplifier before being presented to the transient digitizer, and so the recorded signals consist of peaks that result from when the droplets enter and leave the image charge detection tube (see Figure 1). For a positively charged droplet, the first peak is negative and the second peak is positive, while for a negatively charged droplet, the polarities are reversed. The area under the peaks is proportional to the charge on the droplet, and the separation between the entrance and exit peaks is related to the velocity of the droplet. In a typical experiment, we record transients for 10 000 droplets, and these transients are analyzed

off-line by a computer program that determines the area of each peak and the separation between the entrance and exit peaks. The program discards transients that do not meet strict quality criteria. For example, the program rejects transients that contain baseline fluctuations, transients that contain signals from more than one droplet, and transients where the areas of entrance and exit peaks are significantly different.

The charge measurements are calibrated by injecting a test charge into the input of the preamplifier by means of a voltage pulse and a capacitor. The capacitor consists of seven 6.7 pF (1%) capacitors connected in series. The input voltage pulse is recorded in one channel of the transient digitizer while the processed signal from the differentiating amplifier is recorded in the other. The rise and fall times of the voltage pulse are set to approximately match those for the droplet signals. Both detectors were calibrated in the same way. The accuracy of the calibration is limited primarily by the uncertainty in the capacitance which is, in principle, $1\%/(7)^{1/2} = 0.38\%$.[34] However, in practice, any stray capacitance will provide a systematic error. The calibration of the two detectors can be cross-checked by plotting the charge recorded for a series of droplets in the second detector against the charge recorded in the first. Ideally, this plot should be a perfect straight line with a slope of one and an intercept of zero. In practice, we find there are a few droplets where the charge changes substantially. We attribute this to the droplets discharging or fragmenting between the detectors (see below). When these outliers are removed, we find a good straight line ($r = 0.999\ 92$) with a slope of 0.998 53 and an intercept of 29 elementary charges (e). Thus, the charge obtained from the two detectors agrees to within a fraction of a percent.

The time between the entrance and exit peaks in the transients is related to the velocity of the droplets. In order to convert the time into a velocity, the length of the image charge detection tube must be calibrated. The effective length of the detection tube is slightly longer than the actual length.[23] The calibration is performed by turning off the pulsed accelerator and simultaneously recording transients for the same droplet with both detectors. Since we can measure the distance between the detectors accurately, the velocity of the droplets can then be accurately determined from the time between when the droplet enters the first detector and when it enters the second. This velocity (along with the time difference between the entrance and exit peaks) is then used to determine the effective length of the image charge detection tubes.

RESULTS

Figure 2 shows an example of the transients recorded as a droplet travels through the first and second image charge detectors. In these transients, the first peak is negative, which indicates that the droplet is positively charged. The transients shown in the figure were recorded with the differentiating amplifier time constant set at 3.0 μs and with a gain of 500. The time it takes to travel through the first image charge detector (t_A) is 119.46 μs, and the time through the second (t_B) is 91.94 μs. The decrease in the transit time is due to the acceleration of the droplet in the pulsed accelerator. In this case, the droplet is
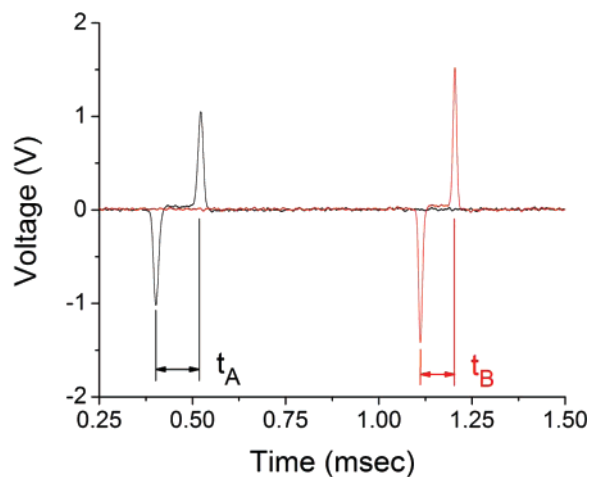
Figure 2. Example of the transients recorded as a droplet travels through the first and second image charge detectors. The first peak is negative, which indicates that the droplet is positively charged. The transients were recorded with the differentiating amplifier time constant set at 3.0 μs and with a gain of 500. t_A is the time it takes to travel through the first image charge detector (119.46 μs), and t_B is the time through the second (91.94 μs).
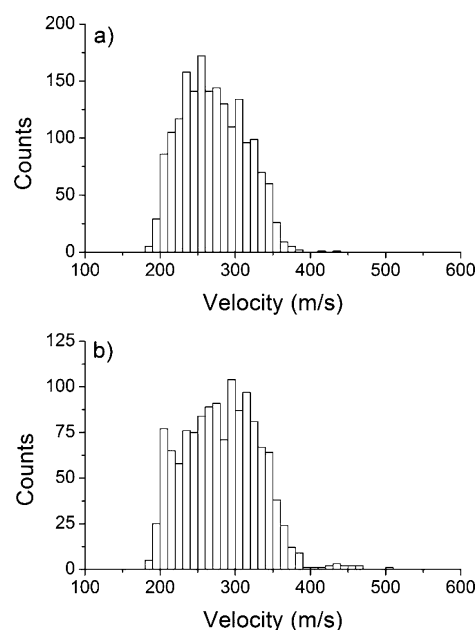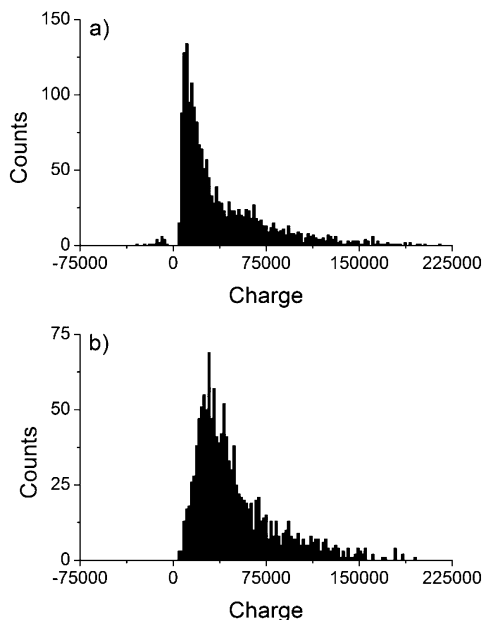

Figure 3. Histograms of the velocities measured for droplets passing through the first detector. The bin size is 10 m/s. Results are shown for positive droplets from positive mode electrospray with (a) the capillary interface and (b) the aperture interface.

accelerated by 101.51 m/s. Along with the decrease in the transit time, the amplitude of the signal in the second detector is larger than in the first. This occurs because the droplet is traveling faster and enters the detector more rapidly. The area under the peaks is proportional to the charge. The charges obtained from the first and second detectors are 44,839 and 45,067 e, respectively. The 0.5% difference between these values is not statistically significant.

Figure 3 shows the velocity distribution recorded with the first image charge detector. Results are shown for positive droplets from positive mode electrospray with (a) the capillary interface and (b) the aperture interface. The distributions are similar, but the distribution obtained with the capillary interface peaks at a slightly lower velocity ($\sim$250 m/s) than the aperture interface

Figure 4. Histograms of the charges measured for droplets passing through the first detector. The bin size is 2,000 e. Results are shown for positive mode electrospray with (a) the capillary interface and (b) the aperture interface.

Figure 5. Histograms showing velocity differences caused by the pulsed accelerator for positive droplets from positive mode electrospray with (a) the capillary interface; and (b) the aperture interface. The bin size is 1 m/s. The results for droplets with velocity changes less than 0.61 m/s are not included (see text).

($\sim$300 m/s). Figure 4 shows charge distributions recorded in the first image charge detector for positive mode electrospray. The charge distribution for the droplets transmitted through the capillary interface (a) shows a peak at $\sim$10 000 e and a tail that extends past 150 000 e. The charge distribution for the droplets transmitted through the aperture interface (b) peaks at $\sim$30 000 e with a tail that extends past 150 000 e. The average charge obtained from the distribution for the capillary interface is 39 626 e while the average charge obtained from the distribution for the aperture interface is 50 466 e. We have noted elsewhere that $\sim$1% of the droplets transmitted through a capillary interface from positive electrospray of water are negatively charged.[35] Negatively charged droplets are not found with the aperture interface; all the droplets are positively charged.

Figure 5 shows histograms of the velocity differences caused by the pulsed accelerator. The accuracy of the velocity differences can be evaluated by comparing the velocities determined in the two detectors with the pulsed acceleration turned off. The mean absolute difference in the velocities, $\overline{\Delta v}$, obtained in this way is 0.61 m/s. Hence, velocity differences less than 0.61 m/s are unreliable, and results for droplets that are accelerated by less than 0.61 m/s are not included in Figure 5. For the capillary interface, almost all of the velocity differences are less than 25 m/s. The distribution of velocity differences obtained with the aperture interface is bimodal with a low velocity component that is similar to the distribution found with the capillary interface and a broad high-velocity component that extends past 125 m/s.

Not all the droplets make it through both detectors. In some cases, the droplets seem to disappear between the detectors—there is a signal in the first detector, but no signal at the appropriate time in the second. We attribute this behavior primarily to the droplet missing the aperture into the second
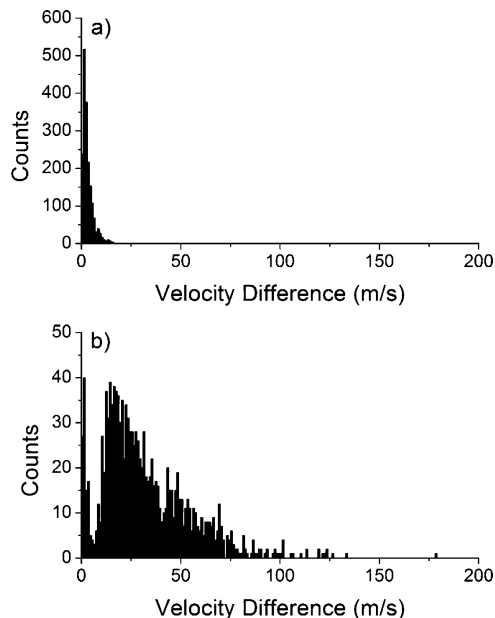
detector. Since the second detector is further from the source, its acceptance angle is smaller, and some droplets that get through the first detector are not able to get through the second on geometric grounds. In some cases, the charge on the droplet changes between the detectors, and in other cases, it appears that the droplets break up between the detectors. In other words, the transient in the first detector indicates a single droplet, while two or more transients are found at the appropriate time in the second detector. We do not include the results for droplets that change charge or break up in Figure 5, or in what follows. This behavior, which is still under investigation, will be discussed elsewhere.

The mass to charge ratio of the droplets can be obtained from the initial and final velocities using[36]

$$m/z = \frac{2eV}{v_\mathrm{f}^2 - v_\mathrm{i}^2} \qquad (1)$$

where V is the acceleration voltage, e is the electronic charge, and v_f and v_i are the final and initial velocities, respectively. Figure 6 shows histograms of the m/z values for droplets transmitted through (a) the capillary interface and (b) the aperture interface. The accuracy of m/z values obtained here is determined by the uncertainty in the velocity measurements. Since $v_\mathrm{f}^2 - v_\mathrm{i}^2 = (v_\mathrm{f} + v_\mathrm{i})(v_\mathrm{f} - v_\mathrm{i})$, the relative uncertainty in the m/z values for small velocity differences is approximately $\overline{\Delta v}/(v_\mathrm{f} - v_\mathrm{i})$, where $\overline{\Delta v}$ is the mean absolute difference in the velocity measurements determined without the pulse accelerator. As noted above, $\overline{\Delta v}$ was found to have a value of 0.61 m/s. Thus, for a velocity

(35) Maze, J. L.; Jones, T. C.; Jarrold, M. F. *J. Phys. Chem. A* **2006**, *110*, 12607–12612.

(36) It is straightforward to derive this equation using conservation of energy: $1/2mv_f^2 = 1/2mv_i^2 + zeV$, where the first term is the final kinetic energy, the second term is the initial kinetic energy (from the aerodynamic acceleration), and the third term is the kinetic energy gained in the pulsed accelerator.
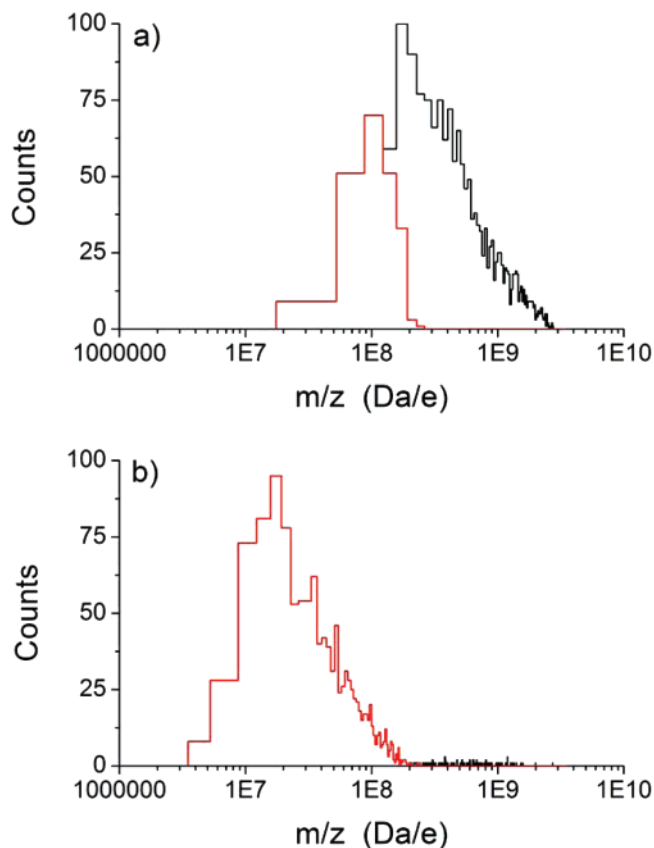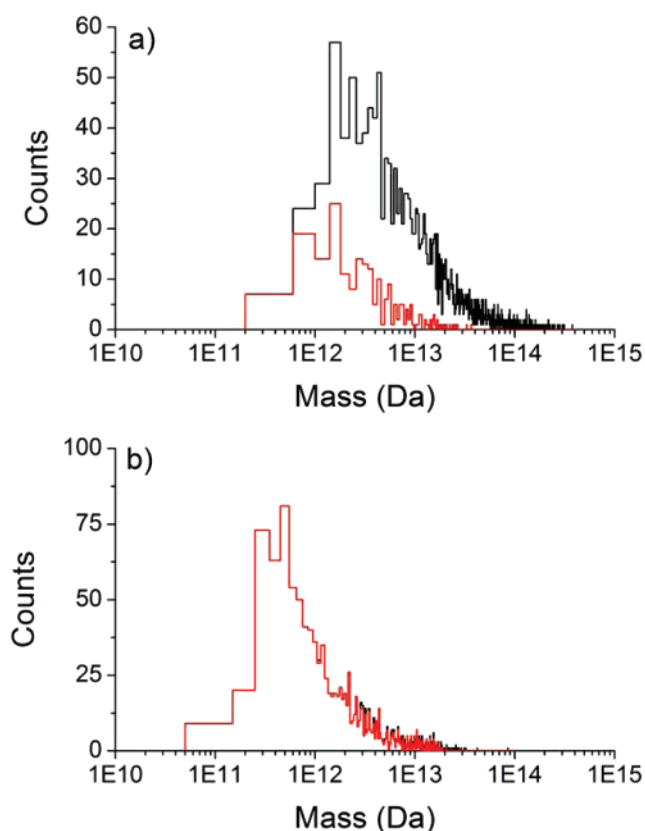
Figure 6. Histograms of the *m/z* ratios (in Da/e) derived for positive droplets from positive mode electrospray with (a) the capillary interface and (b) the aperture interface. The bin size is 3.5×10^7 Da/e in (a) and 3.5×10^6 Da/e in (b). Results are shown for droplets that show velocity changes greater than 6.1 m/s (red histogram) and greater than 0.61 m/s (red and black histograms) (see text).

Figure 7. Histograms of the masses (in Da) derived for positive droplets transmitted through (a) the capillary interface and (b) the aperture interface. The bin size is 4×10^{11} Da in (a) and 1×10^{11} Da in (b). Results are shown for droplets that show velocity changes greater than 6.1 m/s (red histogram) and greater than 0.61 m/s (red and black histograms).

difference, $(v_f - v_i)$, of 61 m/s, the uncertainty in the *m/z* values is 1%. If the velocity difference is 6.1 m/s, the uncertainty increases to 10% and, for velocity differences of less than 0.61 m/s, the *m/z* values become completely unreliable. The red histograms in Figure 6 show the *m/z* values determined with a cutoff in the velocity differences of 6.1 m/s (less than 10% uncertainty in the *m/z* values). As can be seen from the velocity difference distributions in Figure 5, many of the droplets transmitted through the capillary interface have velocity differences less than 6.1 m/s, but most of the droplets transmitted through the aperture interface have larger velocity differences. The black histogram in Figure 6 shows the result of lowering the cutoff in the velocity difference to 0.61 m/s. Lowering the cutoff populates *m/z* values in the $2 \times 10^8 - 2 \times 10^9$ Da/e range. The *m/z* distribution for the droplets from the capillary interface extends from $\sim 2 \times 10^7$ Da/e to over 2×10^9 Da/e. The histogram for the droplets transmitted through the aperture interface extends from around 3×10^6 to 2×10^8 Da/e, with a low-intensity tail that extends to over 10^9 Da/e. The low-intensity tail results from the low-velocity component in the velocity difference distribution (see Figure 5). The *m/z* ratios for the droplets transmitted through the aperture interface are ~ 1 order of magnitude smaller than those transmitted through the capillary interface.

Since the charge is determined for each droplet in the image charge detectors, the *m/z* values for the individual droplets can

be converted into masses by multiplying by the average charge. Cases where the charges determined from the two detectors are significantly different are excluded. The mass distributions are shown in Figure 7. The red histogram shows droplets with velocity differences greater than 6.1 m/s, and the black histogram is obtained by lowering the cutoff in the velocity difference to 0.61 m/s. The masses of the droplets transmitted through the capillary interface are ~ 1 order of magnitude larger than the droplets transmitted through the aperture interface. For droplets with such large masses, it may make more sense to report their radii. Radii were calculated by assuming the droplets are perfectly spherical and by assuming a density of 1 g/cm^3. Histograms of the radii are shown in Figure 8. For the droplets transmitted through the capillary interface, the radii range from ~ 0.6 to ~ 5 μm and peak at ~ 1.5 μm. The droplets transmitted through the aperture interface range in size from ~ 0.3 to ~ 2.0 μm and peak at ~ 0.6 μm. The droplets transmitted through the capillary interface are much larger than those transmitted through the aperture interface. The droplet size distributions reported here represent the distributions for the small fraction of droplets that are on axis and transmitted through the two skimmers. It is possible that the distributions are affected by a sampling bias, and we are currently investigating this issue.

A question we have not yet addressed is whether the droplets carry most of the charge that travels through the image charge detectors or just a small fraction? To answer this question, we
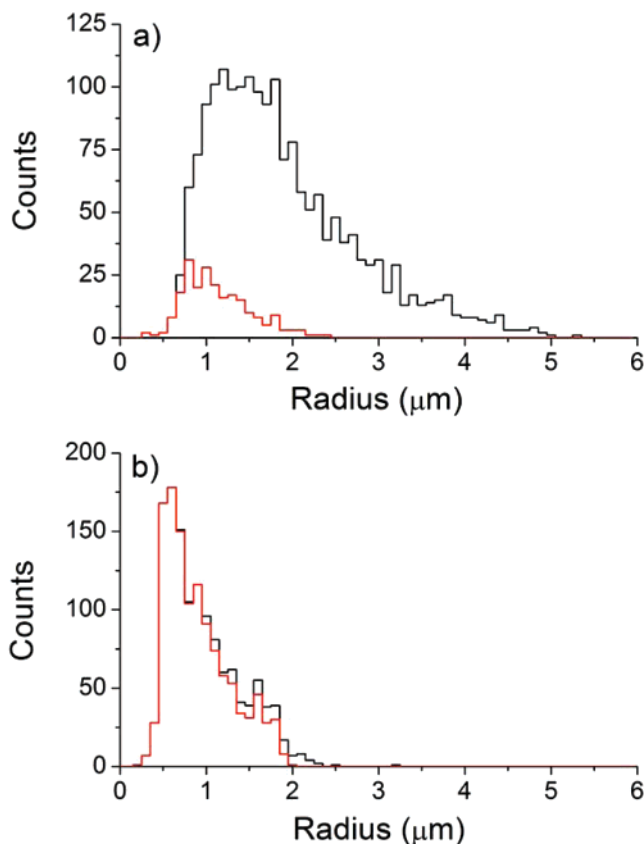
Figure 8. Histograms of the droplet radii (in μm) for positive droplets transmitted through (a) the capillary interface and (b) the aperture interface. The bin size is 0.1 μm. Results are shown for droplets that show velocity changes greater than 6.1 m/s (red histogram) and greater than 0.61 m/s (red and black histograms).

installed a Faraday cup after the first image charge detector and integrated the current on the Faraday cup while the droplets' signals were measured using the first image charge detector. We found that the image charge detector recorded ~20% of the charge measured on the Faraday cup. Thus, 80% of the current on the Faraday cup is from ions with a low charge that are not detected by the image charge detector. This current probably results from small charged water clusters.

DISCUSSION

Accuracy and Limitations of Pulsed Acceleration Charge Detection Mass Spectrometry. The accuracy of the m/z values determined by pulsed acceleration charge detection mass spectrometry is limited by how accurately the velocities can be measured. As noted above, the accuracy of the velocity measurements can be determined by comparing the velocities measured in the two detectors with the pulsed accelerator turned off. The relative uncertainty in the m/z values is then given approximately by $\overline{\Delta v}/(v_f - v_i)$, where $\overline{\Delta v}$ is the mean absolute difference in the velocities determined with the pulsed accelerator turned off. The relative uncertainty increases as the velocity difference decreases. Since $m/z \propto 1/(v_f - v_i)$, the relative uncertainty is $\propto 1/(m/z)$. Under the conditions employed here, the relative uncertainty in the m/z values is ~10% at 10^8 Da/e. The relative uncertainty decreases to 1% at ~10^7 Da/e. However, it will not continue to decrease unchecked. The approach to determining the uncertainty

outlined above is only valid for small velocity differences. For large differences, $v_f \gg v_i$, the accuracy of the m/z values becomes limited by the accuracy of the measurement of the final velocity which is ~0.14%. This could be improved by making the image charge detectors longer. The current experimental configuration should be capable of accurately measuring m/z ratios down to at least 10^3 Da/e.[37]

The accuracy of the mass values is determined by the accuracy of the m/z measurements and the accuracy of the charge measurements. The accuracy of the charge measurements has been discussed above. For large z, it is limited by the accuracy of the charge calibration, which is probably better than 1%. For small z, the accuracy of the charge measurement becomes limited by the signal-to-noise ratio. The current experimental configuration has been used to measure charges between 10^3 and 10^6 e, and the uncertainty in the charge measurements at 10^3 e, due to the noise, is estimated to be ~15%.[38]

We have demonstrated that masses in the $10^{10}-10^{14}$ Da range can be measured using pulsed acceleration charge detection mass spectrometry. We anticipate that the approach can be extended to masses of <10^6 Da.

Comparison with Rayleigh Limit. Charged droplets become unstable when electrostatic forces exceed the surface tension. Rayleigh investigated this instability by considering whether small distortions from spherical were stabilizing or destabilizing.[30,40] This analysis led to the following expression (often called the Rayleigh limit) for the maximum charge that can be carried by a charged droplet:

$$q_R = 8\pi[\epsilon_0 \gamma r^3]^{1/2} \qquad (2)$$

In this equation, q_R is the charge on the droplet at the Rayleigh limit, r is the radius, and μ is the surface energy. Unstable droplets (where $ze > q_R$) may fission into two or more progeny with roughly equal size or discharge by emitting a fine jet of charged nanodroplets.[41-45] The jetting process has been recorded for levitated microdroplets.[41,44,46-48] As noted in the introduction, electrosprayed droplets are thought to evaporate until they reach the Rayleigh limit and then discharge by jetting. Some studies suggest that the discharge event occurs at a charge somewhat below the Rayleigh limit. For example, according to Gomez and Tang, the droplets only reach 70−80% of the Rayleigh limit before discharging.[49]

(37) It may be necessary to lower the voltage in the pulsed accelerator to measure low m/z ratios.

(38) The charge is determined from the size of the steps in the integrated transients. The uncertainty was estimated by comparing the step size to the short-term random fluctuations (which are due to noise).

(39) Deleted in proof.

(40) Hendricks, C. D.; Schneider, J. M. *Am. J. Phys.* **1963**, *31*, 450−453.

(41) Taflin, D. C.; Ward, T. L.; Davis, E. J. *Langmuir* **1989**, *5*, 376−384.

(42) Gomez, A.; Tang, K. *Phys. Fluids* **1994**, *6*, 404−414.

(43) Feng, X.; Bogan, M. J.; Agnes, G. R. *Anal. Chem.* **2001**, *73*, 4499−4507.

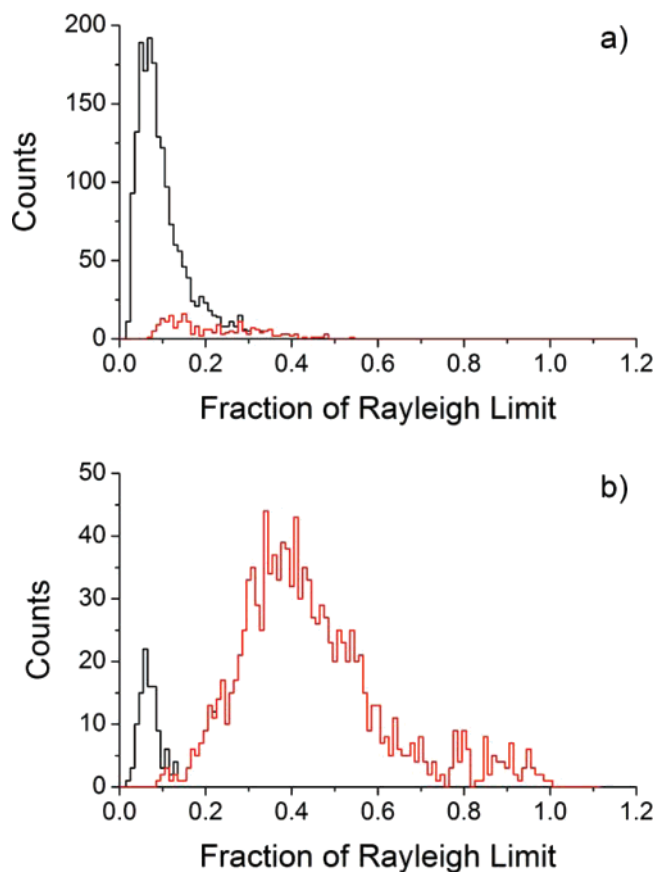(44) Smith, J. N.; Flagan, R. C.; Beauchamp, J. L. *J. Phys. Chem. A* **2002**, *106*, 9957−9967.

(45) Duft, D.; Achtzehn, T.; Muller, R.; Huber, B. A.; Leisner, T. *Nature* **2003**, *421*, 128−128.

(46) Hager, D. B.; Dovichi, N. J. *Anal. Chem.* **1994**, *66*, 1593−1594.

(47) Hager, D. B.; Dovichi, N. J.; Klassen, J. S.; Kebarle, P. *Anal. Chem.* **1994**, *66*, 3944−3949.

(48) Grimm, R. L.; Beauchamp, J. L. *J. Phys. Chem. B* **2005**, *109*, 8244−8250.

(49) Tang, K.; Smith, R. D. *J. Am. Soc. Mass Spectrom.* **2001**, *12*, 343−347.

Figure 9. Histograms of the fraction of the Rayleigh limit (ze/q_R) for positive droplets transmitted through (a) the capillary interface and (b) the aperture interface. The bin size is 0.01. Results are shown for droplets that show velocity changes greater than 6.1 m/s (red histogram) and greater than 0.61 m/s (red and black histograms).

Since we determine the charge and the radius of the droplets, we can investigate how highly they are charged relative to the Rayleigh limit, q_R. Figure 9 shows histograms of the fraction of the Rayleigh limit (ze/q_R) for (a) droplets transmitted through the capillary interface and (b) droplets transmitted through the aperture interface. Most of the droplets transmitted through the capillary interface have ze/q_R values less than 0.2. In other words, the droplets transmitted through the capillary interface are only charged to a small fraction of the Rayleigh limit. The histogram for the aperture interface is bimodal with a low ze/q_R component that appears to correspond to the low ze/q_R values found with the capillary interface. This low ze/q_R component results from the low-velocity component in the histogram of the velocity differences (Figure 5). In addition to the low ze/q_R component for the droplets transmitted through the aperture interface, there is a larger ze/q_R component centered around 0.4, which has a tail that extends to the Rayleigh limit ($ze/q_R = 1$). However, no droplets are charged to significantly above the Rayleigh limit. The low charge found on the droplets transmitted through the capillary interface is the big surprise to come from the comparison of the charges with the Rayleigh limit.

Micrometer-sized water droplets cool rapidly by evaporation in vacuum and given enough time they will supercool and freeze. We have developed a model for this process, which we will describe in detail elsewhere. Based on this model, we expect that

some of the droplets (the small and the slow-moving ones) will freeze before the mass measurements. During the evaporation and freezing process, the droplets will lose ~15% of their volume (i.e., the radius will shrink by ~5%). For droplets that are charged to close to the Rayleigh limit, this shrinkage could trigger a fission or jetting event. However, most of the droplets are charged to only a fraction of the Rayleigh limit.

It has been known for some time that neutral droplets can be distorted and disrupted by a strong electric field.[50] The disruption occurs at a critical field called the Taylor limit:

$$E_c = \frac{C}{(8\pi)^{1/2}} \left(\frac{2\gamma}{\epsilon_0 r}\right)^{1/2} \tag{3}$$

In this expression, c is a constant with a value of 1.625 for liquid droplets in air. For a water droplet with a radius of 1 μm, the Taylor limit is 4.2×10^7 V/m. However, Grimm and Beauchamp[48] have shown that charged droplets discharge at a lower field than the Taylor limit. The Taylor limit for a 1-μm droplet (4.2×10^7 V/m) is over 1 order of magnitude larger than the field employed in the pulsed accelerator (2.2×10^6 V/m). However, the field in the pulsed accelerator could still cause the discharge of droplets that are charged near to the Rayleigh limit. To investigate this possibility, we have measured the droplet charges and masses with a configuration that employs fields that are 1 order of magnitude smaller than employed in the pulsed accelerator described here. The results were not significantly different, which indicates that the droplets do not discharge in the pulsed accelerator.

Implications for the Mechanism of Electrospray Ionization. A surprising feature of the measurements reported here is the relatively low charge on the droplets from the capillary interface (~10% of the Rayleigh limit). This could be due to the droplets discharging on the walls of the capillary. However, there are two arguments against this. First, if the droplets are colliding with the capillary walls, why are they not completely discharged? Second, for all the droplets to collide with the capillary walls (they all have a low charge), the flow through the capillary must be turbulent, but there is reason to believe that it is laminar. If we raise the temperature of the capillary interface to 100 °C, many of the droplets survive. This can only occur under laminar flow conditions, where the heat transfer from the walls to the center of the capillary is slow compared with the time that it takes for the droplets to travel through the capillary.

The low charge on the droplets transmitted through the capillary interface does not appear to be consistent with the idea that they break up through a series of Rayleigh jetting processes. One interpretation of this result is that aerodynamic forces in the capillary interface contribute to the break up. For example, laminar flow through the capillary results in a hyperbolic velocity gradient that may be strong enough to spin-up the droplets so that the resulting centrifugal force contributes to their breakup.

The observation that the droplets observed from the aperture interface are 1 order of magnitude smaller in mass than those found with the capillary interface is also unexpected. The longer residence time in the capillary interface might be expected to lead

(50) Taylor, G. *Proc. R. Soc. London A* **1964**, *280*, 383–397.
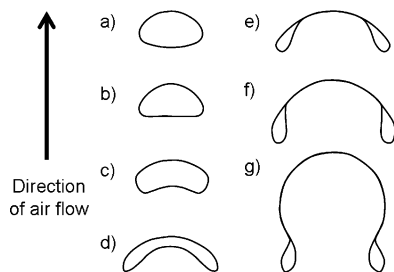
Figure 10. Mechanism of the aerodynamic breakup of millimeter-sized water droplets. The diagrams show cross sections through the droplet as it breaks- p. Adapted from ref 52.

to smaller droplets. While it remains possible that the mass distributions are affected by a sampling bias, this observation can also be rationalized by the aerodynamic forces in the vacuum interfaces.

In the aperture interface, the transition from atmospheric pressure to vacuum is abrupt, and in the resulting expansion, there is initially, at least, a large difference between the velocity of the droplet and the velocity of the surrounding air, leading to a strong aerodynamic force on the droplet.

Photographs of the aerodynamic breakup of millimeter-sized droplets show that it occurs through the bubble-bursting mechanism illustrated in Figure 10.[51,52] First, the droplet flattens and then a bubble, supported by a toroidal ring, forms. Eventually, the bubble bursts releasing numerous small droplets, and then the ring breaks up into a smaller number (tens) of large droplets. The aerodynamic force required to blow up and burst a droplet in this way increases with decreasing droplet size. According to Lane,[51] velocities of $300-400$ m/s are needed to disrupt uncharged micrometer-sized water droplets. Larger velocities than this probably occur in the expansion at the aperture interface. Furthermore, the force required to distort a charged droplet must be smaller than for an uncharged droplet. So this is a plausible breakup mechanism for the charged droplets in the aperture interface.[53]

With the capillary interface, the droplets are accelerated by the capillary flow before they enter the expansion at the end of the capillary. Thus, the aerodynamic forces on the droplets in the expansion at the end of the capillary interface are substantially smaller than in the aperture interface. Hence, the breakup of the droplets by the bubble-bursting mechanism is probably less important.

SUMMARY

We have described a new approach to charge detection mass spectrometry consisting of two charge detectors separated by a pulsed acceleration stage. The main advantage of this approach is that it takes into account the ions initial translational energy. The method has been used to measure the masses of individual macroions in the $10^{10}-10^{14}$ Da range with $z = 10^3-10^6$ and $m/z = 10^6-10^9$. The uncertainty in the mass measurements is $\sim$10% at 10^{14} Da, but drops to $\sim$0.1% at $<10^{12}$ Da. We are currently working on improving the accuracy of the mass measurements and anticipate that it can be employed for ions with masses of $<10^6$ Da.

We have measured the size and charge of electrosprayed water droplets transmitted through a capillary interface and an aperture interface. We find that the droplets transmitted through the aperture interface are much smaller that those transmitted through a capillary interface. This result is consistent with the droplets being broken up in the aperture interface by the strong aerodynamic forces in the expansion. We find that the charge on the droplets transmitted through the capillary interface is remarkably low—$\sim$10% of the Rayleigh limit. The cause of this low charge is not obvious. It is possible that the aerodynamic forces in the capillary, in particular the large shear rate, cause the droplets to spin so that centrifugal forces contribute to their breakup. Regardless of the explanation, the results suggest that the evolution of charged droplets in an electrospray source is more complex and more interesting than previously believed. We are planning experiments where we inject well-characterized single-sized droplets into the interfaces to gain more insight into how they break up.

(51) Lane, W. H. *Ind. Eng. Chem.* **1951**, *43*, 1312−1317.
(52) Matthews, J. B.; Mason, B. J. *Q.. J. R. Met. Soc.* **1964**, *90*, 275−286.
(53) Maze, J. T.; Zilch, L. W.; Mabbett, S. R.; Smith, J. W.; Ewing, G. E.; Jarrold, M. F. *J. Phys. Chem. A* (submitted).